

Supporting Information

Duetting electronic structure modulation of Ru atoms in RuSe₂@NC enables more moderate H* adsorption and water dissociation for hydrogen evolution reaction

Ding Chen,^{a,b#} Ruihu Lu,^{c#} Youtao Yao,^{a#} Dulan Wu,^a Hongyu Zhao,^a Ruohan Yu,^a Zonghua Pu,^a Pengyan Wang,^a Jiawei Zhu,^a Jun Yu,^a Pengxia Ji,^a Zongkui Kou,^{a} Haolin Tang,^{a,b*} Shichun Mu^{a,b*}*

^a State Key Laboratory of Advanced Technology for Materials Synthesis and Processing, Wuhan University of Technology, Wuhan 430070, China.

^b Foshan Xianhu Laboratory, Foshan 528200, China.

^c State Key Laboratory of Silicate Materials for Architectures, International School of Materials Science and Engineering, Wuhan University of Technology, Wuhan 430070, China.

E-mail: zongkuikou@whut.edu.cn, thln@whut.edu.cn, msc@whut.edu.cn

1. Experimental Details

1.1 Computational Details

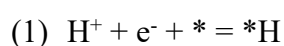
All DFT calculation were constructed and implemented in the Vienna ab initio simulation package (VASP).[1,2] Using the electron exchange and correlation energy was treated within the generalized gradient approximation in the Perdew-Burke-Ernzerhof functional (GGA-PBE),[3] the calculations were done with a plane-wave basis set defined by a kinetic energy cutoff of 450 eV. The k -point sampling was obtained from the Monkhorst-Pack scheme with a $(3 \times 3 \times 1)$ mesh for optimization and a $(5 \times 5 \times 1)$ mesh for the calculations of electronic structure. The geometry optimization and energy calculation are finished when the electronic self-consistent iteration and force were reach 10^{-5} eV and 0.02 eV \AA^{-1} , respectively.

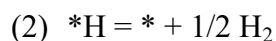
Models

The RuSe₂ slab was modeled from the RuSe₂ (001) plane. The RuSe₂ supercell with a lattice constant of $12.02 \times 12.02 \text{ \AA}^2$ is consisted of 80 atoms with 3 layers separated by a vacuum region of 15 Å along the direction normal to the sheet plane to avoid strong interactions. During optimization, the bottom layer is fixed and the upper two adjacent layers is free without fixed coordination. For building the RuSe₂@NC model, we integrate 2 layers RuSe₂ with 1 layer N-doping graphene to construct a heterolayer in box with a lattice constant of $12.16 \times 12.41 \text{ \AA}^2$, which comprises of 91 atoms.

HER

The HER process is divided into the four fundamental reactions as following:





*H presents the H moiety on the adsorption site. Where which the energy of H⁺/e⁻ is approximately equal to the energy of 1/2 H₂. [4]

The Gibbs Free Energy Variation

The change in Gibbs free energy (ΔG) of each adsorbed intermediate is calculated based on the computational hydrogen electrode method developed by Nørskov et al. At standard condition ($T = 298.15 \text{ K}$, $\text{pH} = 0$, and $U = 0 \text{ V}$ (vs. SHE)), the free energy G is defined as the following equation:

$$\Delta G = \Delta E + \Delta E_{\text{ZPE}} - T\Delta S$$

Where ΔE is the energy change obtained from DFT calculation, ΔE_{ZPE} is the difference between the adsorbed state and gas, which was calculated by summing vibrational frequency for all model based on the equation: $E_{\text{ZPE}} = 1/2 \sum h\nu_i$. T is the temperature (298.15 K) in the above reaction system, and ΔS represents the difference on the entropies between the adsorbed state and gas phase. The entropies of free molecules were obtained from NIST database (<https://janaf.nist.gov/>). And the free energy of the adsorbed state *H can be taken as: $\Delta G_{\text{*H}} = \Delta E_{\text{*H}} + 0.24$. [5]

***d*-band center**

The *d*-band center proposed by Nørskov and co-workers [6] is a semi-quantitative descriptor to describe the trend of reactivity of transition metals (TM), which is defined the *d*-band center (ϵ_d) relative to the Fermi level (EF). A transition metal with a low ϵ_d value relative to the Fermi level, shows a weak adsorption for a given adsorbate. And the ϵ_d is calculated as following:

$$\varepsilon_d = \frac{\int_{-\infty}^{+\infty} x\rho(x)dx}{\int_{-\infty}^{+\infty} \rho(x)dx}$$

Predicted HER polarization curve

The HER polarization curve is calculated using the turnover frequency (TOF) and the number of active sites, where:

$$\text{TOF} = \frac{\text{total number of H}_2 \text{ atoms per second}}{\text{total number of active sites per unit area}}$$

As previously reported,[7] we take the TOF of Pt as a benchmark for Arrhenius type equation, where we utilized the *H adsorption energy and an active site density of N_{as} .

The current density j can be calculated as following:

$$j = 2qN_{\text{as}} \times \text{TOF}$$

where $q = 1.6 \times 10^{-19}$ C is the elementary charge and 2 is the number of atoms per H_2 .

1.2 Materials and Reagents

Ruthenium (IV) oxide (RuO_2) was purchased from Wokai Reagents Ltd. Selenium powder (Se) and chitosan were obtained from Aladdin Reagents Ltd. Anhydrous lithium chloride (LiCl), potassium chloride (KCl), potassium hydroxide (KOH), sulfuric acid (H_2SO_4), absolute ethanol and isopropyl alcohol were purchased from Sinopharm Chemical Reagent Co., Ltd. Commercial Pt/C (20 wt%) and Nafion (5 wt%) were obtained from Sigma-Aldrich. All the reagents are analytical grade and used without further treatment. Deionized (DI) water was employed as solvent.

1.3 Material Syntheses

For a typical synthesis, 1 mmol of RuO_2 , 2 mmol of Se powder and 500 mg chitosan are mixed with 2.5 g of a mixture for the eutectic salt KCl-LiCl ($n_{\text{KCl}}: n_{\text{LiCl}} =$

41 : 59) and ground under exclusion of water and oxygen into a fine powder. Then mixture was added into a corundum boat and heated for 4 hours at 600 °C under inert atmosphere. After cooled to room temperature, the black product was collected, washed by centrifugation with alcohol and water several times to remove the residue of reactants, and finally dried in vacuum at 60 °C overnight. Finally, the product of RuSe₂@NC was obtained. Furthermore, the NC and pure RuSe₂ samples as benchmark were also synthesized , respectively, by the same method with or without adding chitosan.

1.4 Material Characterization

X-ray diffraction (XRD) patterns were collected on a Rigaku X-ray diffractometer equipped with a Cu *K* α radiation source to obtain the crystalline structure of all samples. X-ray photoelectron spectrometer (XPS) was carried out to reveal the elemental composition and electronic structure. The morphology and structure were characterized by double spherical aberration-corrected scanning transmission electron microscope (AC-STEM, Titan Cubed Themis G2 300).

1.5 Electrochemical Measurements

All electrochemical measurements were performed in a conventional three-electrode system at room temperature using a CHI 660E electrochemical analyzer (CHI Instruments, Shanghai, China). The electrochemical measurements were performed using a Hg/HgO and a graphite plate as the reference electrode and the counter electrode, respectively. The catalyst ink was prepared by dispersing 5 mg as-prepared sample into a mixture (900 μ L isopropyl alcohol, 100 μ L water and 20 μ L 5% Nafion

solution) and ultrasonic dispersion for 40 min. For comparison, 5 mg commercial catalyst powder (20 wt% Pt/C) was evenly dispersed into the same mixture. Polarization data were obtained at a scan rate of 5 mV s⁻¹. All polarization curves were iR-corrected. The electrochemical impedance spectroscopy (EIS) was conducted at the corresponding potentials of 10 mA cm⁻² from LSV curves, with the frequency range of 0.01 Hz to 100 kHz with AC amplitude of 10 mV. The electrochemical double layer capacitance (C_{dl}) was determined with typical cyclic voltammetry (CV) measurements at various scan rates (20, 40, 60, 80 and 100 mV s⁻¹) in nonreactive region. The turnover frequency (TOF) values for HER are calculated from following equations: $TOF = j \cdot A / 2 \cdot n \cdot F$, where j is the current density estimated from the LSV, A stand for the exposed area of applied electrode, F is the Faraday constant and n is the number of moles of metal content in the electrode. The durability was evaluated by comparing LSV curves before and after CV cycling test and chronoamperometry at the overpotential of 10 mA cm⁻².

2. Supplementary Figures and Tables

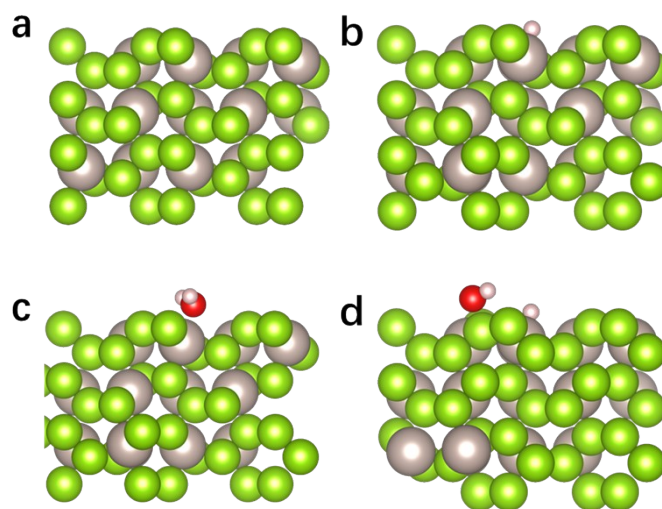


Figure S1. Schematic diagram of RuSe₂ with none (a), *H (b), *H₂O (c) and *H+*OH (d), respectively. Where the white, red, green and pink denote the H, O, Se and Ru atoms.

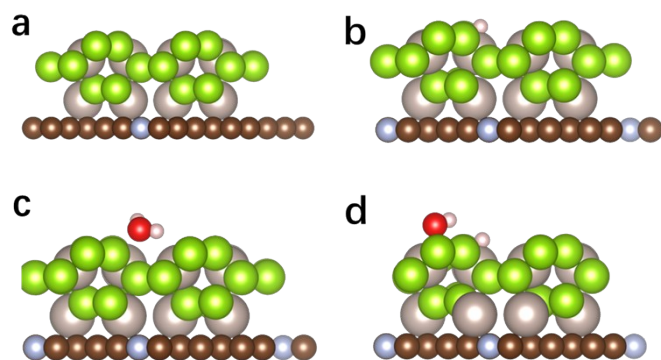


Figure S2. Schematic diagram of RuSe₂@NC with none (a), *H (b), *H₂O (c) and *H+*OH (d), respectively. where the white, grey, blue, red, green and pink denote the H, C, N, O, Se and Ru atoms.

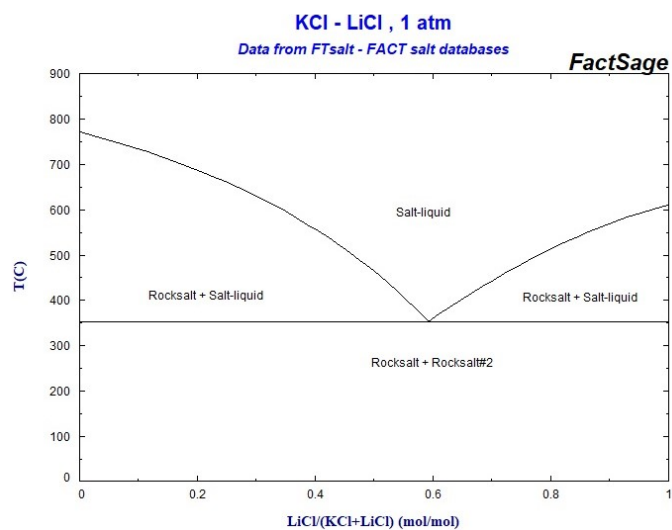


Figure S3. The phase diagram of the two-salt system (KCl + LiCl), which coming from the <http://www.crct.polymtl.ca/FACT/documentation/> (FTsalt → KCl-LiCl).

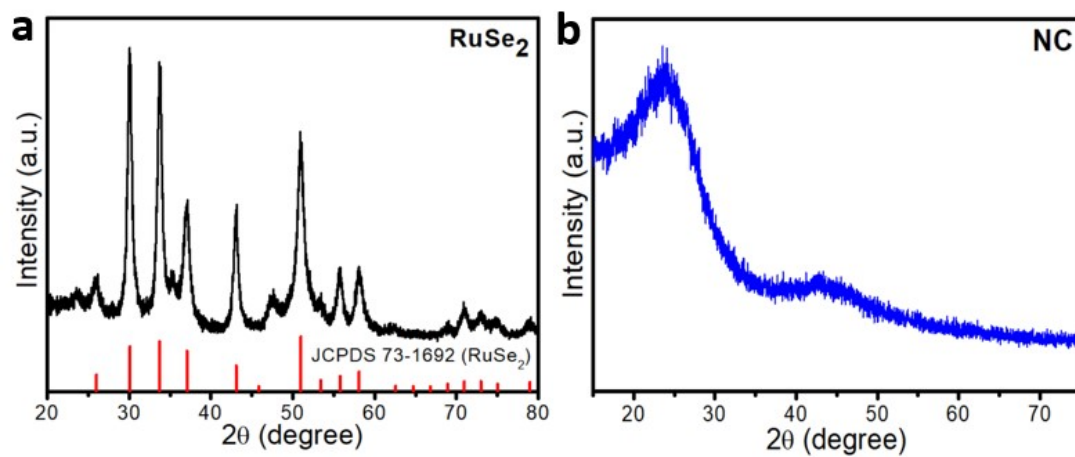


Figure S4. (a) XRD patterns of pure (a) RuSe₂ and (b) NC.

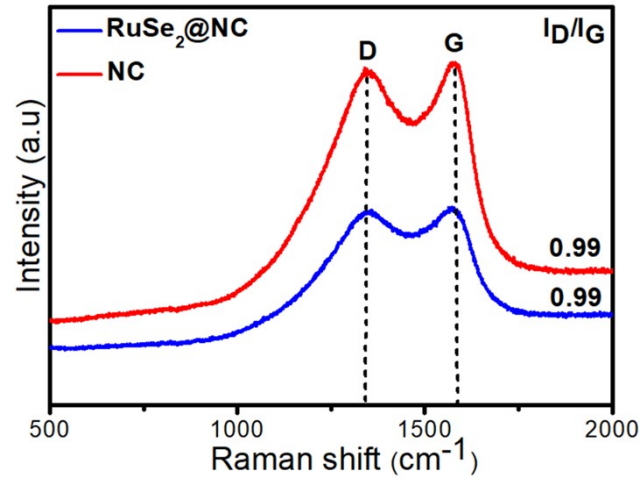


Figure S5. Raman spectra of RuSe₂@NC and NC.

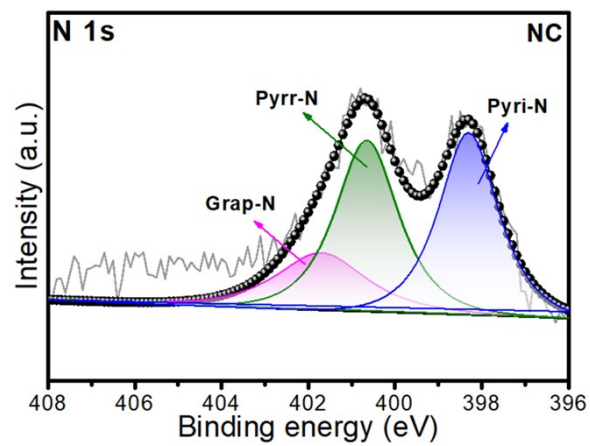


Figure S6. N 1s spectra of pure NC.

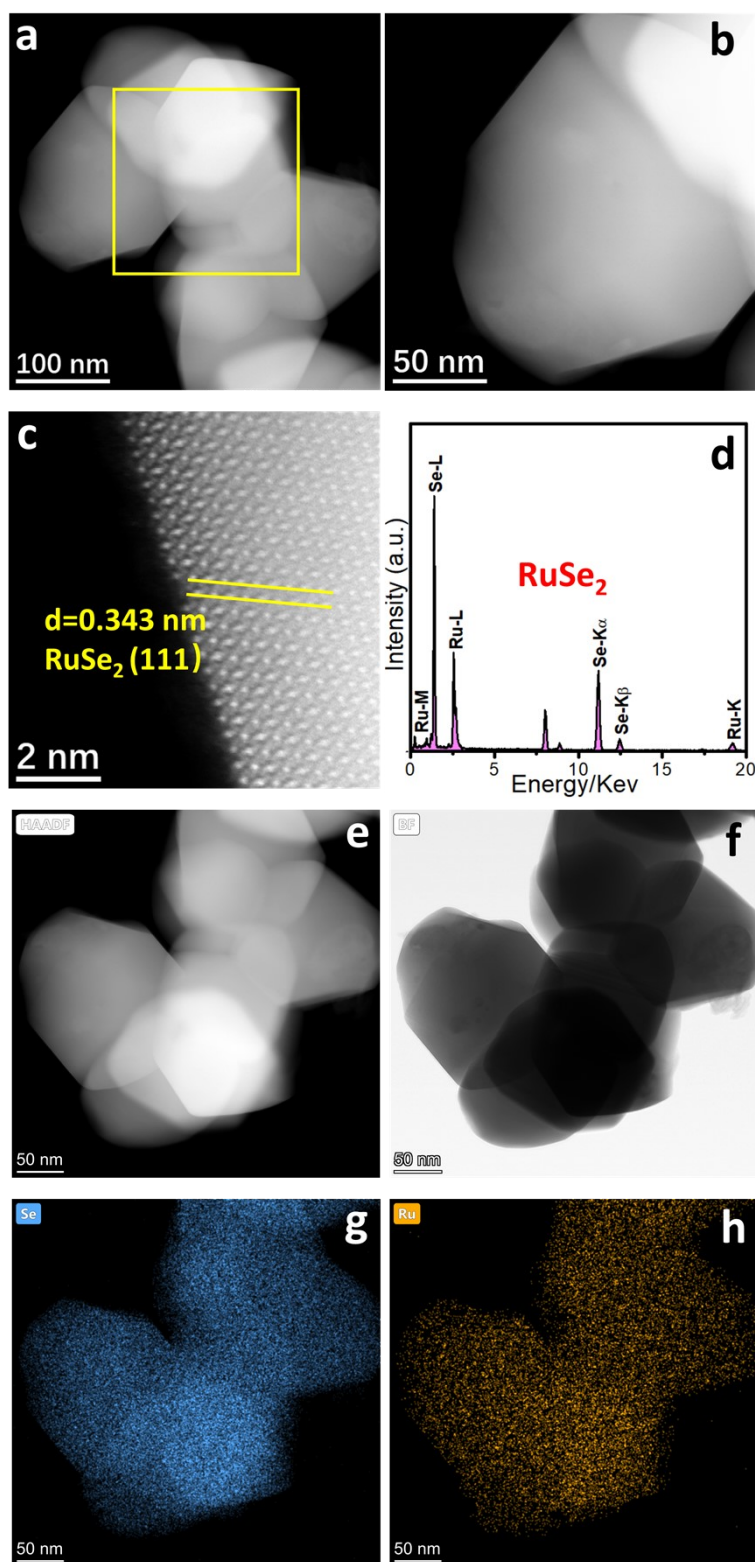


Figure S7. (a-c) STEM images of pure RuSe₂. (d) EDS composition of RuSe₂ from the area indicated by the yellow box in (a). (e) HAADF, (f) BF images and corresponding elemental distribution for (g) Se and (h) Ru of RuSe₂.

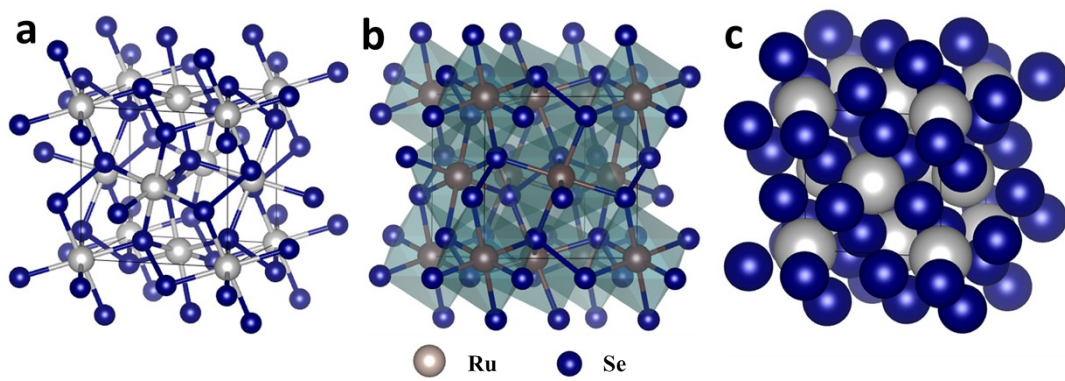


Figure S8. (a) Ball-and-stick, (b) polyhedral and (c) space-filling crystal structure of RuSe₂.

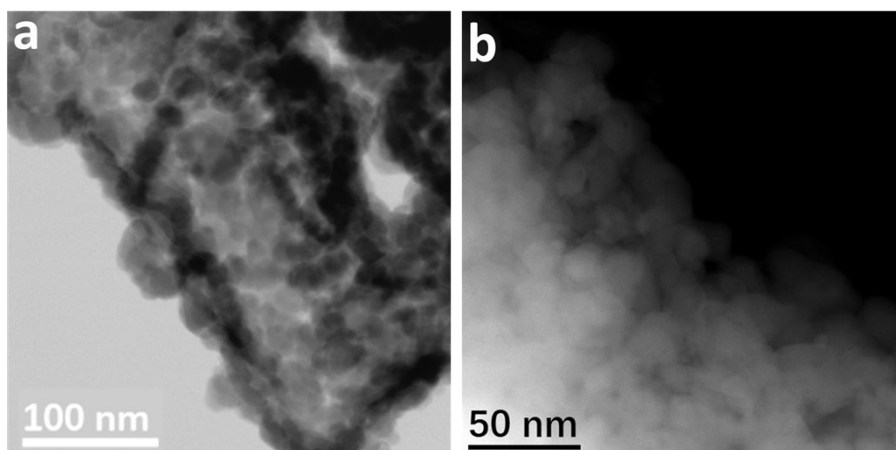


Figure S9. (a) The corresponding BF images of **Figure 4a**. (b) STEM image of RuSe₂@NC.

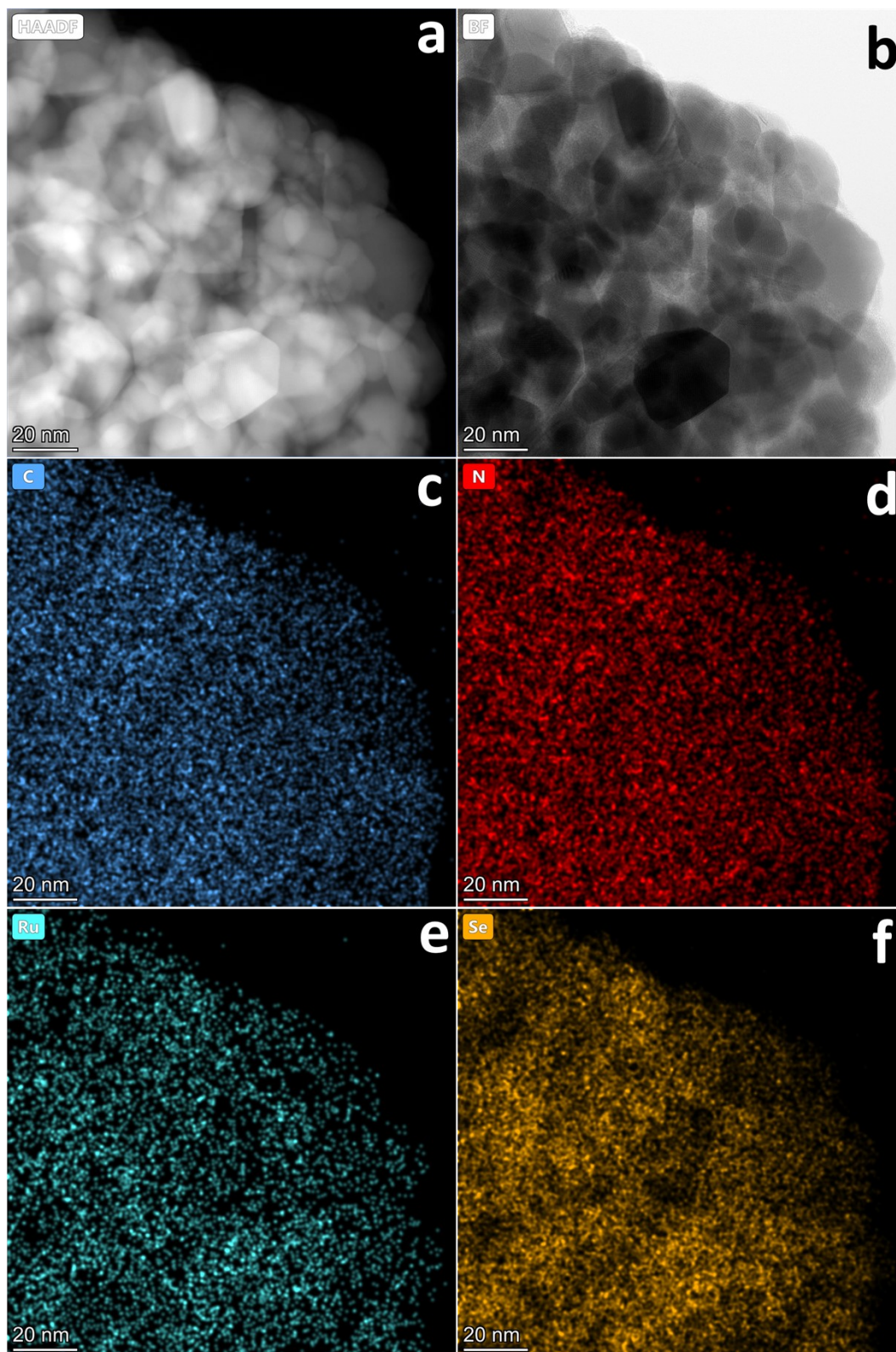


Figure S10. (a) HAADF, (b) BF images and corresponding elemental distribution for (c) C, (d) N, (e) Ru and (f) Se of RuSe₂@NC.

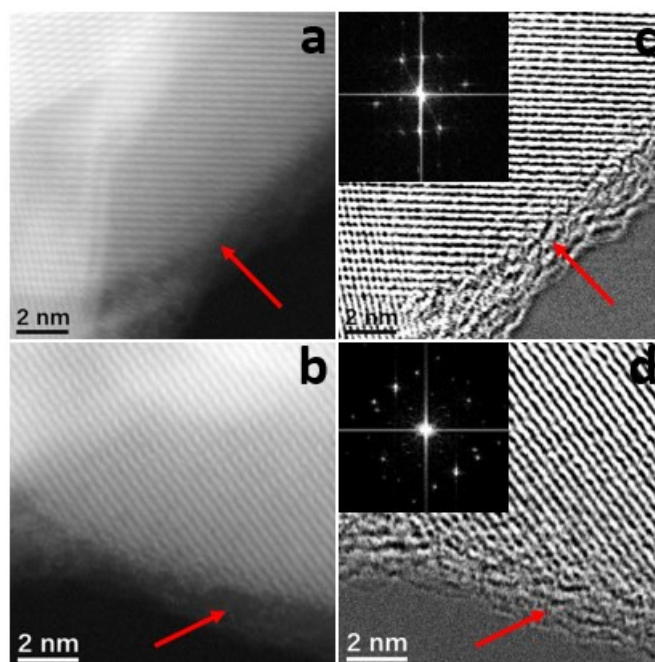


Figure S11. (a, b) and (c, d) HAADF and BF images of corresponding edge areas in RuSe₂@NC. Inset: corresponding FFT pattern from (c) and (d).

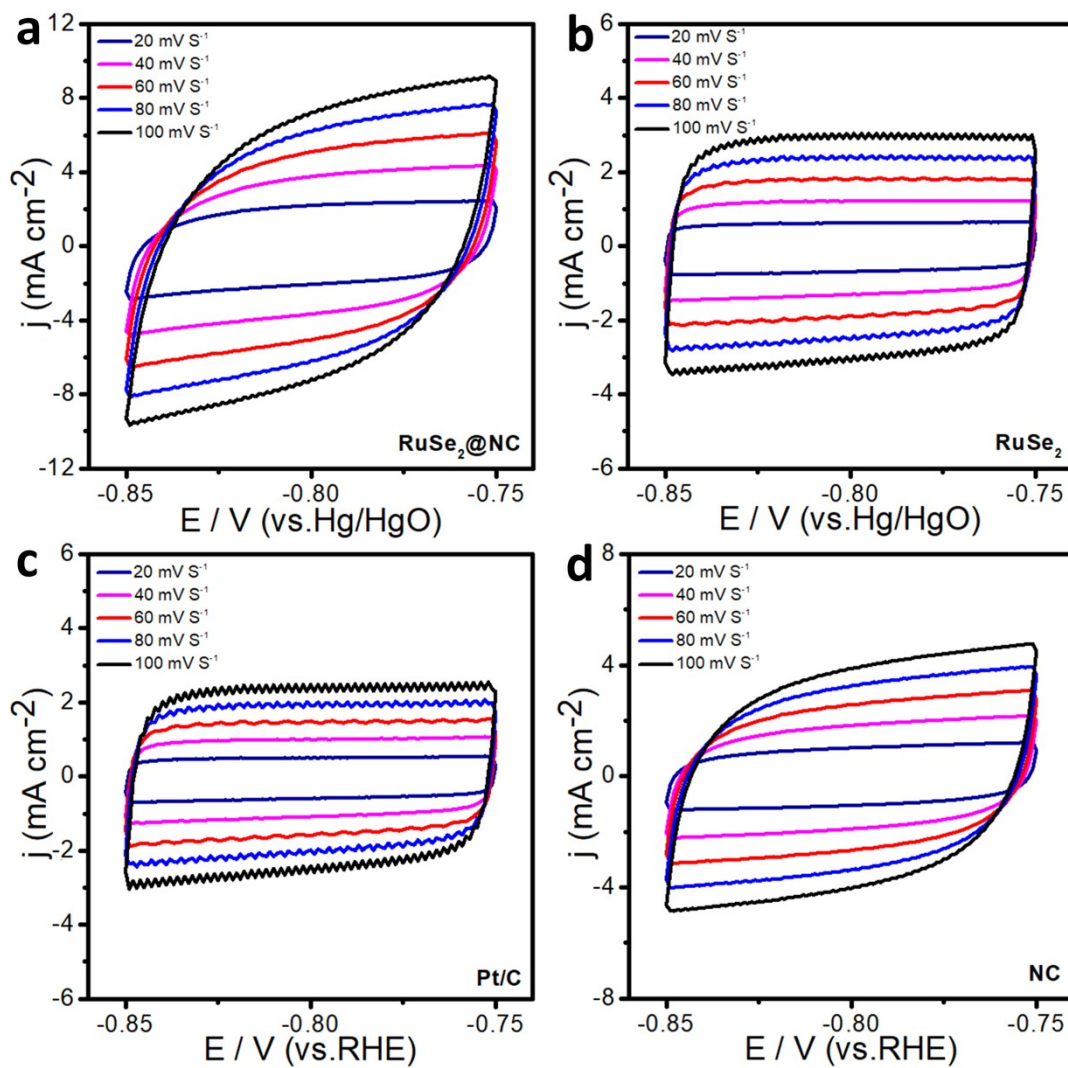


Figure S12. Cyclic voltammograms of (a) RuSe₂@NC, (b) RuSe₂, (c) Pt/C and (d) NC in the region of (-0.85) - (-0.75) V versus Hg/HgO at different scan rates.

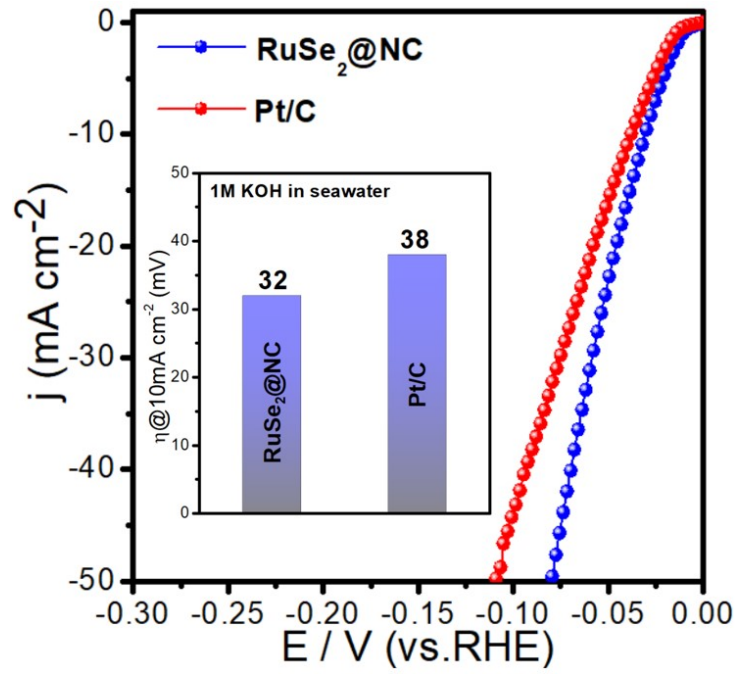


Figure S13. HER polarization curves of RuSe₂@NC and commercial Pt/C in alkaline simulated seawater.

Table S1. Comparison of HER performance of RuSe₂@NC with other reported Ru-based electrocatalysts in 1 M KOH.

Catalyst	Overpotential@j (mV @ mA cm ⁻²)	reference
RuSe ₂ @NC	30@10	This work
Commercial Pt-C	36@10	This work
RhSe ₂	81.6@10	<i>Adv. Mater.</i> 2021 , 33, 2007894
RuS ₂ @NPC/CNT	54.5@10	<i>Small</i> 2021 , 17, 2007333
Ni@Ni ₂ P-Ru	43@10	<i>J. Am. Chem. Soc.</i> 2018 , 140, 2731.
RuNi/CQDs	13@10	<i>Angew. Chem. Int. Ed.</i> 2020 , 59, 1718-1726
PdP ₂ @CB	35.5@10	<i>Angew. Chem. Int. Ed.</i> 2018 , 57,14862-14867
IrP ₂ @NPC	42@10	<i>J. Mater. Chem. A</i> , 2021 , 9, 2195
Li-IrSe ₂	72@10	<i>Angew. Chem. Int. Ed.</i> 2019 , 58, 14764-14769
OsP ₂ @NPC	70@10	<i>Journal of Catalysis.</i> 370 (2019) 404-411
Rh ₂ P	30@10	<i>Adv. Energy Mater.</i> 2018 , 8, 1703489
RuP ₂ @NPC	52@10	<i>Angew. Chem. Int. Ed.</i> 2017 , 56, 11559-11564
Ru@CN-0.16	32@10	<i>Energy Environ. Sci.</i> 11, 800-806 (2018)
a-RuTe ₂ PNRs	36@10	<i>Nat Commun</i> 10, 5692 (2019)
Ru/C ₃ N ₄ /C	79@10	<i>J. Am. Chem. Soc.</i> 2016 , 138, 16174.

Reference

- [1] Efficiency of ab-initio total energy calculations for metals and semiconductors using a plane-wave basis set. ([https://doi.org/10.1016/0927-0256\(96\)00008-0](https://doi.org/10.1016/0927-0256(96)00008-0))
- [2] Efficient iterative schemes for ab initio total-energy calculations using a plane-wave basis set. (<https://doi.org/10.1103/PhysRevB.54.11169>)
- [3] Generalized gradient approximation to the angle- and system-averaged exchange hole. (<https://doi.org/10.1063/1.476928>)
- [4] Origin of the Overpotential for Oxygen Reduction at a Fuel-Cell Cathode. (<https://doi.org/10.1021/jp047349j>)
- [5] Trends in the exchange current for hydrogen evolution. (<https://doi.org/10.1149/1.1856988>)
- [6] Density functional theory in surface chemistry and catalysis. (<https://doi.org/10.1073/pnas.1006652108>)
- [7] Prediction of Enhanced Catalytic Activity for Hydrogen Evolution Reaction in Janus Transition Metal Dichalcogenides. (<https://doi.org/10.1021/acs.nanolett.8b01335>)